

# The Generalized Carrier-Greenspan Transform for the shallow water system with arbitrary initial and boundary conditions

Alexei Rybkin<sup>1</sup>

Dmitry Nicolsky<sup>2</sup>

Efim Pelinovsky<sup>3,4,5</sup>

Maxwell Buckel<sup>1</sup>

<sup>1</sup>Department of Mathematics and Statistics, University of Alaska Fairbanks, USA

<sup>2</sup>Geophysical Institute, University of Alaska Fairbanks, USA

<sup>3</sup>National Research University - Higher School of Economics, Moscow, Russia

<sup>4</sup>Institute of Applied Physics, Nizhny Novgorod, Russia

<sup>5</sup>Nizhny Novgorod State Technical University n.a. R.E. Alekseev, Nizhny Novgorod, Russia

August 26, 2020

## Abstract

We put forward a solution to the initial boundary value (IBV) problem for the nonlinear shallow water system in inclined channels of arbitrary cross-section by means of the generalized Carrier-Greenspan hodograph transform (Rybkin et al., 2014). Since the Carrier-Greenspan transform, while linearizing the shallow water system, seriously entangles the IBV in the hodograph plane, all previous solutions required some restrictive assumptions on the IBV conditions, e.g., zero initial velocity, smallness of boundary conditions. For arbitrary non-breaking initial conditions in the physical space, we present an explicit formula for equivalent IBV conditions in the hodograph plane, which can readily be treated by conventional methods. Our procedure, which we call the method of data projection, is based on the Taylor formula and allows us to reduce the transformed IBV data given on curves in the hodograph plane to the equivalent data on lines. Our method works equally well for any inclined bathymetry (not only plane beaches)

and, moreover, is fully analytical for U-shaped bays. Numerical simulations show that our method is very robust and can be used to give express forecasting of tsunami wave inundation in narrow bays and fjords<sup>1</sup>.

## 1 Introduction

Walter Craig made an outstanding contribution towards development of nonlinear theories of the long wave dynamics in fluids of the variable depths (Craig and Groves, 1994; Craig et al., 2004, 2005b,a; Craig, 2006; Craig and Wayne, 2007). Here we present a new solution of the nonlinear shallow-water equations for long waves, tsunamis, in the inclined channels of variable depth. As a motion of viscous fluid, tsunami waves are described by the Navier-Stokes equations, a highly nonlinear 3+1 (three spatial and one temporal derivatives) system, which is notoriously hard to analyze even numerically. However, in many important cases some extra assumptions lead to considerable simplifications. For instance, assuming that depth/wavelength, wave height/depth are small and truncating the Taylor expansions of nonlinear terms produce a whole zoo of approximations commonly called shallow water equations (e.g. Korteweg–de Vries, Boussinesq, Saint–Venant, to name just three). Further assumptions that the vertical velocity is small and no vorticity effectively reduce the Navier–Stokes equations to the (2+1) shallow water-wave equations (SWE) which provide an accurate model for predicting tsunami wave behavior (Synolakis, 1991; Synolakis and Bernard, 2006; NTHMP, 2012; Kanoglu et al., 2015; Kanoglu and Synolakis, 2015). Still, for general bathymetries this model allows us to analyze tsunami wave run-ups (our main concern) only numerically (for an analytical solution for a specific bathymetry see (Synolakis et al., 2008)). For a complete analysis of tsunami hydrodynamics, modeling, and forecasting, we refer the reader to Kanoglu et al. (2015); Pelinovsky (2006); Madsen et al. (2008), and Synolakis and Bernard (2006). Mathematically rigorous treatment of SWE including the well-posedness and exact solutions can be found in Dobrokhotov and Tirozzi (2010); Dobrokhotov et al. (2010, 2013), Alekseenko et al. (2017) and references therein. It is worth mentioning that IVP for SWE have been treated in Chugunov et al. (2014, 2020) using a perturbation approach.

We make five additional assumptions: the wave is long (i.e. the height/length ratio is small), friction and dispersion are both negligible, the bathymetry (see Figure 1a) has the main axis located along  $x$  and is uniformly inclined. The SWE then reduce further to the 1+1 system (also called

---

<sup>1</sup>To appear in *Water Waves* (2020)

shallow water)(Stoker, 1957; Lannes, 2013), which in dimension units and standard notation reads

$$\begin{cases} \partial_t S + \partial_x(Su) & = 0 & \text{(continuity equation)} \\ \partial_t u + u\partial_x u + g\partial_x \eta & = 0 & \text{(momentum equation)} \end{cases}, \quad (1)$$

where:

- $\eta(x, t)$  is the water elevation over unperturbed water level  $z = 0$ . It need not be sign definite (can be positive or negative).
- $u(x, t)$  is the flow velocity averaged over the cross-section. Since the positive  $x$ -axis is directed off-shore,  $u < 0$  and  $u > 0$  corresponds respectively to an in-coming wave (i.e. moving towards the shore) and out-going wave (i.e. moving from the shore).
- $S(x, t)$  is the cross-section area corresponding to the total water depth  $H(x, t) = h(x) + \eta(x, t)$  along the main axis  $x$  (see Figure 1b). Here  $h(x)$  is the distance between the hard bottom given by  $z = -h(x)$  (along the main axis  $x$ ) and the unperturbed water level  $z = 0$ . Note that  $h(x) < 0$  if  $x < 0$ , and the shoreline location  $x_s$  at the head of the bay is defined by  $H(x_s, t) = h(x_s) + \eta(x_s, t) = 0$ .

We have assumed that our bathymetry (bay for short) is inclined. We agree to call a bay *inclined* if

$$h(x) = \alpha x, \quad \alpha > 0, \quad S(x, t) = S(H(x, t)), \quad dS/dH > 0. \quad (2)$$

In other words, it has a constant slope and  $S(x, t)$  depends on  $(x, t)$  only via  $H(x, t)$ . This is the case when the equation for the bottom is given by

$$z(x, y) = -\alpha x + f(y) \quad (3)$$

with some  $f \geq 0$ . Clearly, for a bay with one main axis  $f(y) = 0$  if and only if  $y = 0$ . The unperturbed shoreline along the bay is given by  $f(y) - \alpha x = 0$ .

- $g$  is the acceleration due to gravity.

Note that while our bay is seemingly 3-D, its geometry is described by only one single variable function  $S(H)$  (or  $f(y)$ ). That is why the system (1) for two unknown functions  $\eta$  and  $u$  is essentially 1+1.

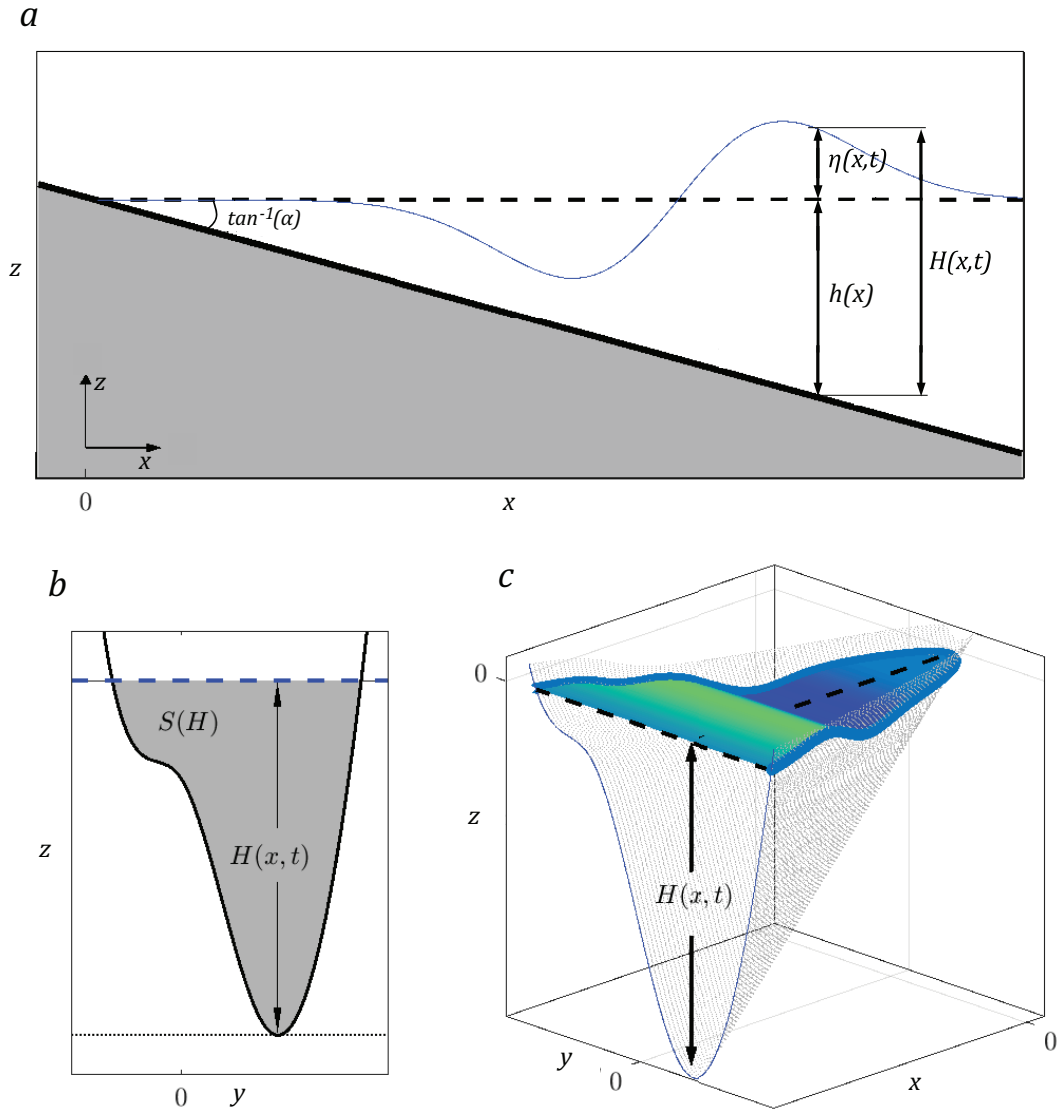


Figure 1: A: An  $xz$  cross-section along the main axis of the bay. Both the unperturbed  $h(x)$  (dashed black) and perturbed  $H(x,t)$  (solid blue) water levels are displayed. B:  $yz$  cross-section of a generic bay. Both  $H(x,t)$  (dashed blue) and the cross-sectional area  $S(H)$  (shaded area) are displayed. C: a 3-D view of the uniformly sloping bay, which cross-section is displayed in plot B.

In this paper we are concerned with the initial boundary value problem (IBVP) for (1). That is, both  $\eta$  and  $u$  are specified at the initial instant of time:

$$\eta(x, 0) = \eta_0(x), \quad u(x, 0) = u_0(x). \quad (4)$$

We will refer to such initial conditions (IC) as standard IC. Such IC naturally occur, among others, in the study of tsunami waves generated by landslides and near shore earthquakes. As a boundary condition (BC) we take

$$\eta(l, t) = \eta_b(t), \quad u(l, t) = u_b(t), \quad (5)$$

where  $l$  is a fixed point  $l > 0$ . Such BC appear e.g. in the study of finite bathymetries and piece-wise inclined bays (see below). Typically,  $\eta_b(t)$  and  $u_b(t)$  cannot be set up independently. As a matter of fact, it is already the case for subcritical flows ( $u^2 < gH$ ). We refer the interested reader to Antuono and Brocchini (2007, 2010) for extensive discussions on how to set up “correct” BC in this case and algorithms for solving IBVP for (1) based on perturbation technics. Note that the assumption that the flow is subcritical is hard to enforce at the dry/wet boundary. Our considerations, on the other hand, do not need this assumption. The price to pay is that we need both  $\eta_b(t)$  and  $u_b(t)$ . However, this set-up is not unrealistic as it would correspond, e.g., to the problem of computing the wave in a bay by measuring (in real time) the water displacement and velocity flow at a fixed point  $x = b$ .

It is convenient to go in (1) over to dimensionless units  $\tilde{x}, \tilde{t}, \tilde{\eta}, \tilde{u}$  defined from

$$x = (H_0/\alpha) \tilde{x}, \quad t = \sqrt{H_0/g} \tilde{t}/\alpha, \quad \eta = H_0 \tilde{\eta}, \quad u = \sqrt{H_0 g} \tilde{u}, \quad (6)$$

where  $H_0$  is a typical (characteristic) height. Substituting (6) into (1)-(4) and rewriting the first equation in (1) using (2), we have (omitting the tilde)

$$\left\{ \begin{array}{l} \partial_t \eta + (1 + \partial_x \eta) u + c^2 (x + \eta) \partial_x u = 0 \\ \partial_t u + u \partial_x u + \partial_x \eta = 0 \\ \eta(x, 0) = \eta_0(x) \\ u(x, 0) = u_0(x) \\ \eta(l, t) = \eta_b(t) \\ u(l, t) = u_b(t) \end{array} \right. , \quad (7)$$

where

$$c^2(x) := S(H_0 x) / H_0 S'(H_0 x) \geq 0. \quad (8)$$

The classical example of such idealized bathymetry is the plane infinite beach (i.e. extending along the  $y$  axis infinitely far). In this case, as one can easily see, (7) takes the specifically simple form

$$\begin{cases} \partial_t \eta + \partial_x [(x + \eta) u] = 0 \\ \partial_t u + u \partial_x u + \partial_x \eta = 0 \end{cases}. \quad (9)$$

The system (9) has a quadratic nonlinearity. What is remarkable about it is that the substitution

$$\varphi(\sigma, \tau) = u(x, t), \quad \psi(\sigma, \tau) = \eta(x, t) + u^2(x, t)/2, \quad \text{new unknowns}, \quad (10a)$$

$$\sigma = x + \eta(x, t), \quad \tau = t - u(x, t), \quad \text{new variables}, \quad (10b)$$

turns it into

$$\begin{cases} \partial_\tau \psi + \sigma \partial_\sigma \varphi + \varphi = 0 \\ \partial_\tau \varphi + \partial_\sigma \psi = 0 \end{cases}, \quad (11)$$

which is a linear hyperbolic system! This substitution (in a slightly different form) was introduced in the seminal paper by Carrier and Greenspan (1958) and is now referred to as the Carrier-Greenspan (CG) transform. The form (10a)-(10b) is taken from Tuck and Hwang (1972). The system is typically written as one equation

$$\partial_\tau^2 \psi = \sigma \partial_\sigma^2 \psi + \partial_\sigma \psi \quad (\text{or } \partial_\tau^2 \varphi = \sigma \partial_\sigma^2 \varphi + 2 \partial_\sigma \varphi), \quad (12)$$

which is the wave equation with variable coefficients (also known in mathematical physics as Klein-Gordon equation). Observe that  $(\sigma, \tau)$  can be viewed as a hodograph plane and thus, conceptually, the CG transform is a hodograph type transform (also called the Carrier-Greenspan hodograph) that turns the nonlinear SWE (7) into the linear wave equation (12), which can, in turn, be explicitly solved by the Hankel transform techniques for a variety of waveforms. This way both boundary value (e.g. Synolakis, 1987; Antuono and Brocchini, 2007, 2010) and initial value problems (IVP) (e.g. Carrier et al., 2003; Kanoglu, 2004; Kanoglu and Synolakis, 2006) have been extensively analyzed. A tremendous amount of information about the SWE was learned this way (in particular, the important nonlinear process of the run-up and run-down of long waves on the coast).

Same approach can be applied to more complicated inclined bays  $S(H)$  (Zahibo et al., 2006). For  $f(y) \sim y^2$  (parabolic bays) equation (12) is the standard (constant coefficient) 1+1 wave equation and hence can be solved by the d'Alembert formula (Didenkulova and Pelinovsky, 2011a). For an arbitrary power bay ( $f(y) \sim |y|^m$ ,  $m > 0$ , which corresponds to  $S(H) \sim H^{(m+1)/m}$ ) there is no d'Alembert solution but a similar to (12) equation takes place, which can be solved by the

very same techniques (Garayshin et al., 2016) as for the plane beach. Note that the plane beach corresponds to  $m = \infty$ . The case  $m < 1$  exhibits a new striking phenomenon: there may be more than one run-up/run-down.

More recently, the CG transform was generalized to inclined bathymetries of arbitrary cross-section (Rybkin et al., 2014). In Raz et al. (2018) we finally show that the very same substitution (10a)-(10b) brings (1) to the linear system

$$\begin{cases} \partial_\tau \psi + c^2(\sigma) \partial_\sigma \varphi + \varphi = 0 \\ \partial_\tau \varphi + \partial_\sigma \psi = 0 \end{cases}, \quad (13)$$

where  $c(\sigma)$  solely encodes the information about the shape of our bay. The system (13) easily implies

$$\partial_\tau^2 \psi = c^2(\sigma) \partial_\sigma^2 \psi + \partial_\sigma \psi. \quad (14)$$

Thus, surprisingly enough, the transformation (10a)-(10b) is universal for all inclined bathymetries and on the hodograph plane (11) and (13) (or (12) and (14)) differ by the speed of propagation  $c(\sigma)$  only. For power-shaped bays  $S(H) \sim H^{(m+1)/m}$  we immediately have  $c^2(\sigma) = \frac{m}{m+1}\sigma$ . In particular, if  $m = \infty$  (plane beach) then  $c^2(\sigma) = \sigma$  and (14) turns into (12) as expected. Only for power bays can (14) be solved in terms of special functions. For all other shapes (14) can effectively be solved and analyzed numerically. See Harris et al. (2016, 2015) and Raz et al. (2018) where detailed analysis is done for trapezoidal, L, W, and other shapes. We also refer to Anderson et al. (2017) for some extensions to piece-wise inclined power bays.

We emphasize that in the original SWE (7) the shoreline  $x_s$  is moving and it is the main problem with its analysis. On the hodograph plane that point corresponds to the fixed point  $\sigma = 0$ . Note that  $c^2(0) = 0$  and hence the differential operation on the right hand side of (14) is singular. It is not a real issue from the mathematical point of view but rather a strong manifestation of nonlinear effects of run-up/run-down. This is one of the main (if not the main) advantages of the CG transform.

The CG transform however has some serious drawbacks. For the reader's convenience we explain in some detail what the issue is. Note first, that the independent variable  $(\sigma, \tau)$  defined by (10b) depend on the independent variable  $(\varphi, \psi)$  defined by (10a). This circumstance would not be an issue if the system (10a) was linear. But the second equation in (10a) has a quadratic nonlinearity and this is the real problem (which, on the bright side, gives fodder for extensive research). The reason is that the IC (4) on the hodograph plane is no longer standard. As Johnson (1997)

simply puts it, “interchanging the dependent and independent variables simplifies the governing equations, but complicates the boundary/initial conditions.” Indeed, under the transformation (10b), the (horizontal) line  $t = 0$  in the physical plane  $(x, t)$  becomes the parametric curve  $\Gamma = (x + \eta_0(x), -u_0(x))$  in the  $(\sigma, \tau)$  plane. From the first equation in (10b) one has  $x = \gamma(\sigma)$ , where  $\gamma$  is the inverse function of  $x + \eta_0(x)$  (i.e. solves the equation  $x + \eta_0(x) = \sigma$ ). Thus

$$\Gamma = \begin{pmatrix} \sigma \\ -u_0|_{\gamma(\sigma)} \end{pmatrix}, \quad \sigma \geq 0 \quad (15)$$

is the curve in the hodograph plane where the IC are specified. From (10a) we immediately have the transformed IC

$$\begin{pmatrix} \varphi \\ \psi \end{pmatrix} \Big|_{\Gamma} = \begin{pmatrix} u_0 \\ \eta_0 + u_0^2/2 \end{pmatrix} \Big|_{\gamma(\sigma)}, \quad \sigma \geq 0. \quad (16)$$

Similarly, the BC (5) transform as follows. Let  $\gamma_b(\tau)$  be the inverse function of  $\tau(t) = t - u_b(t)$  and

$$\Gamma_b = \begin{pmatrix} l + \eta_b|_{\gamma_b(\tau)} \\ \tau \end{pmatrix}, \quad \gamma_b(\tau) \geq 0. \quad (17)$$

Then the BC in the hodograph plane are

$$\begin{pmatrix} \varphi \\ \psi \end{pmatrix} \Big|_{\Gamma_b} = \begin{pmatrix} u_b \\ \eta_b + u_b^2/2 \end{pmatrix} \Big|_{\gamma_b(\tau)}, \quad \gamma_b(\tau) \geq 0. \quad (18)$$

We can now see from (15) that  $\Gamma$  is a horizontal line  $(\sigma, 0)$  if and only if the initial velocity  $u_0 = 0$ . While the latter is an important case, it is also quite restrictive, as we cannot always assume that a tsunami wave is standing sill at the initial instant of time! If  $u_0 \neq 0$  then the IC (16) is no longer standard and the system (13) (and hence the original SWE (7)) cannot be solved in closed form. Same issue of course takes place with (17):  $\Gamma_b$  is a vertical line if and only if  $\eta_b(\gamma_b(\tau)) = \text{const.}$  These issues were already noticed in (Carrier and Greenspan, 1958) and since then it has been a good open problem how to make the CG transform run for general IVP. The main problem is that the curves  $\Gamma$  and  $\Gamma_b$  also depend on IC  $(\eta_0, u_0)$  and BC  $(\eta_b, u_b)$ . This problem has drawn much attention but still only partial answers under various assumptions of the relative smallness of the IC (e.g. Carrier et al., 2003; Kanoglu and Synolakis, 2006; Antuono and Brocchini, 2007, 2010) are available and only in the context of the plane beach. We will discuss these papers in some detail in the main body of the text.



In the current paper, we put forward a complete solution to this problem for arbitrary inclined bays. Our approach goes as follows<sup>2</sup>. By the recipes discussed above, reduce the (nonlinear) SWE problem (7) to the linear system (13) with IC (16) and BC (18) and write it in matrix form

$$\begin{cases} \partial_\tau \Phi + A(\sigma) \partial_\sigma \Phi + B\Phi = 0 \\ \Phi|_\Gamma = \Phi_0(\sigma) \\ \Phi|_{\Gamma_b} = \Psi_0(\tau) \end{cases}, \quad (19)$$

where

$$A(\sigma) = \begin{pmatrix} 0 & 1 \\ c^2(\sigma) & 0 \end{pmatrix}, \quad B = \begin{pmatrix} 0 & 0 \\ 1 & 0 \end{pmatrix}, \quad (20)$$

$$\Phi = \begin{pmatrix} \varphi \\ \psi \end{pmatrix}, \quad \Phi_0(\sigma) = \begin{pmatrix} \varphi_0(\sigma) \\ \psi_0(\sigma) \end{pmatrix}, \quad \Psi_0(\tau) = \begin{pmatrix} \varphi_b(\tau) \\ \psi_b(\tau) \end{pmatrix}$$

and

$$\begin{aligned} \varphi_0(\sigma) &:= u_0(\gamma(\sigma)), & \psi_0(\sigma) &:= \eta_0(\gamma(\sigma)) + \varphi_0^2(\sigma)/2 \\ \varphi_b(\tau) &:= u_b(\gamma_b(\tau)), & \psi_b(\tau) &:= \eta_b(\gamma_b(\tau)) + \varphi_b^2(\tau)/2 \end{aligned}$$

Given accuracy  $\varepsilon$  (could be arbitrarily small), we apply our *method of data projection*, put forward first in our recent Nicolsky et al. (2018) to find new standard IC  $\Phi|_{\tau=0} = \Phi_n(\sigma)$  given explicitly by

$$\Phi_n = \Phi_0 + \sum_{k=1}^n \frac{1}{k!} \varphi_0^k (D^{-1} \Delta)^k \Phi_0, \quad (21)$$

where  $n$  is chosen to satisfy the accuracy  $\varepsilon$ , and ( $I$  is a 2x2 unit matrix)

$$D(\sigma) = I + \varphi_0'(\sigma) A(\sigma), \quad \Delta = -A(\sigma) \frac{d}{d\sigma} - B. \quad (22)$$

We call  $\Phi_n$  the  $n^{\text{th}}$  projection of IC defined on a curve onto the real line. In a similar fashion we find  $\Psi_n$ , projections of BC on some vertical line  $(\sigma_0, \tau)$ , e.g.  $\sigma_0 = l + \eta_0(l, 0)$  to be compatible with the IC. Note that  $n$  in the projections of IC and BC need not be the same. One can now find the solution  $\tilde{\Phi}$  of the standard IVP

$$\begin{cases} \partial_\tau \Phi + A(\sigma) \partial_\sigma \Phi + B\Phi = 0 \\ \Phi|_{\tau=0} = \Phi_n(\sigma) \\ \Psi|_{\sigma=\sigma_0} = \Psi_n(\tau) \end{cases},$$

by any suitable method. Performing the inverse CG transform solves the original problem (7) in the physical space. The latter is, in general, not explicit but can easily be done numerically without

---

<sup>2</sup>We outline the main results here in Introduction. The derivations are given in the main text.

affecting the total accuracy, which remains  $O(\varepsilon)$ . In fact, we can call our method exact as the error it introduces can be made negligible comparing with the one inherited by the shallow water approximation leading to the very SWE (7).

Loosely speaking, the idea behind our method is to replace the IVP we cannot solve with an equivalent one we can. We however emphasize that our equivalent IC/BC would be very hard to guess. The reader is invited to amuse him/herself with trying to unzip (21) even for  $n = 1$ . It was the matrix form (19) that made our derivation quite transparent.

Extensive numerical verification and simulations in Section 5 show that our method is very robust and can be effectively used for rapid forecasting of characteristics of the inundation zone. We will try to make our paper as self-contained as possible.

## 2 The method of data projection

In this section we introduce our *method of data projection* in independent terms and most general situation (e.g.  $(x, t)$  are not as in SWE (1) but rather  $(\sigma, \tau)$ , etc.). We consider projections for IC and BC separately.

### 2.1 Initial value problem

Consider the hyperbolic system

$$\partial_t U = A(x) \partial_x U + B(x) U, \quad (23)$$

where  $U(x, t)$  is an  $m$  column of dependent variables and  $A(x)$  and  $B(x)$  are  $m \times m$  matrices independent of  $t$ . The domain for  $(x, t)$  is inessential for our consideration. Let  $U$  be specified on some curve

$$\Gamma = \{(x, \tau(x))\} \quad (24)$$

in the  $(x, t)$  domain. Set up the following IVP

$$\begin{cases} \partial_t U = A(x) \partial_x U + B(x) U \\ U|_{\Gamma} = U_0(x) \end{cases}, \quad (25)$$

where  $U_0(x)$  is a known function.

Note that we have not imposed any boundary conditions (BC) as we do not actually intend to solve (25) in this section. Thus we assume that (25) is supplemented by suitable BC. Conditions on  $\tau(x)$  and  $U_0(x)$  will be given later.

If  $\tau(x) = 0$  then (25) becomes the standard IVP solvable by a variety of classical techniques which all break down if  $\tau(x) \neq 0$ . Our idea is, given accuracy  $\varepsilon$ , find standard IC  $U|_{t=0} = \tilde{U}_0$  such that the solution  $\tilde{U}$  to

$$\begin{cases} \partial_t U = A\partial_x U + BU \\ U|_{t=0} = \tilde{U}_0(x) \end{cases} \quad (26)$$

would be within  $O(\varepsilon)$  from the actual solution to (25) for all  $(x, t)$  in the domain of interest. I.e. the IVP (25) and (26) are equivalent up to  $O(\varepsilon)$ .

We call the map  $U_0 \rightarrow \tilde{U}_0$  the *projection of the data*  $U_0 = U|_{\Gamma}$  *onto the real line*. The reason why we can call it projection will be clear below from figure 2.

**Remark 1** *It is important feature of our method of data projection, that by the very construction both  $U$  and  $\tilde{U}$  solve (exactly) the same equation (23) but satisfy different (equivalent) IC conditions. Of course  $U$  and  $\tilde{U}$  can be made as close as one wishes (while  $U_0$  and  $\tilde{U}_0$  need not be close at all).*

To construct  $\tilde{U}_0$  we start out with applying the Taylor formula in one variable  $t$  to the solution (still unknown)  $U(x, t)$  of (23). For each fixed point  $(x, t)$  we then have

$$U(x, 0) = \sum_{k=0}^n \frac{1}{k!} \partial_t^k U(x, t) (-t)^k + E_n(x, t) \quad (27)$$

with some error  $E_n$ . I.e., we fix  $(x, t)$  and apply the Taylor formula to the point  $(x, 0)$  and not the other way around. Note that the right hand side of (27) is independent of  $t$  (because  $t = 0$  in left hand side). Taking in (27)  $t = \tau(x)$  yields

$$U|_{t=0}(x) = \sum_{k=0}^n \frac{(-\tau(x))^k}{k!} \left[ \partial_t^k U(x, t) \right] \Big|_{\Gamma} + E_n|_{\Gamma}.$$

Introduce

$$U_n(x) := \sum_{k=0}^n \frac{(-\tau(x))^k}{k!} \left[ \partial_t^k U(x, t) \right] \Big|_{\Gamma}, \quad (28)$$

which we call *the  $n^{\text{th}}$  order projection* of initial data  $U|_{\Gamma}$  onto the real line. We can now claim that if we are able to compute all  $\left[ \partial_t^k U(x, t) \right] \Big|_{\Gamma}$  via  $U_0 = U|_{\Gamma}$  and  $A, B$  then  $U_n$  produces a desirable

standard IC  $\tilde{U}_0$  from (26). Indeed, given error  $\varepsilon$  (no matter how small), we take  $n$  so large as  $|E_n| < \varepsilon$  everywhere in the domain of interest for  $(x, t)$  and hence

$$U|_{t=0} = U_n + O(\varepsilon).$$

Thus the solution  $\tilde{U}$  to (26) with  $\tilde{U}_0 = U_n$  will coincide with the solution  $U$  of (25) up to  $O(\varepsilon)$ .

So, it remains to compute the Taylor coefficients in (28). The zeroth one is obvious

$$U_0(x) = U(x, t)|_\Gamma$$

and it is the data in (25). We call it the 0<sup>th</sup> order projection of the data  $U_0 = U|_\Gamma$  onto the real line. All other Taylor coefficients in (28) can also be explicitly computed. Start with the first one. Restricting (23) to  $\Gamma$ , suppressing the variable, and introducing the convenient short-hand notation

$$\Delta U := (A\partial_x + B)U,$$

we have

$$(\partial_t U)|_\Gamma = (\Delta U)|_\Gamma = A(\partial_x U)|_\Gamma + BU|_\Gamma. \quad (29)$$

Compute now  $(\partial_x U)|_\Gamma$ . To avoid possible confusion, note that  $(\partial_x U)|_\Gamma \neq \frac{d}{dx}(U|_\Gamma)$  (indeed,  $(\partial_x U)|_\Gamma = (\partial_x U)|_{t=\tau(x)}$  whereas  $\frac{d}{dx}(U|_\Gamma) = \frac{d}{dx}U(x, \tau(x))$ ). By the chain rule (prime denotes  $d/dx$ )

$$\begin{aligned} \frac{d}{dx}(U|_\Gamma) &= \frac{d}{dx}U(x, \tau(x)) \\ &= (\partial_x U)|_\Gamma + (\partial_t U) \tau' \quad (\text{by the chain rule}) \\ &= (\partial_x U)|_\Gamma + \{A(\partial_x U)|_\Gamma + BU|_\Gamma\} \tau' \quad (\text{by (29)}) \\ &= (I + \tau' A) (\partial_x U)|_\Gamma + \tau' BU|_\Gamma \\ &= D (\partial_x U)|_\Gamma + \tau' BU|_\Gamma, \end{aligned}$$

where  $I$  is the unit matrix and

$$D := I + \tau' A.$$

Thus,

$$\frac{d}{dx}(U|_\Gamma) = D (\partial_x U)|_\Gamma + \tau' BU|_\Gamma$$

and hence, solving this equation for  $(\partial_x U)|_\Gamma$ , we have

$$\begin{aligned} (\partial_x U)|_\Gamma &= D^{-1} ((U|_\Gamma)' - \tau' BU|_\Gamma) \\ &= D^{-1} (I d/dx - \tau' B) U|_\Gamma. \end{aligned}$$

Substituting this equation into (29) yields

$$\begin{aligned}
(\partial_t U)|_\Gamma &= AD^{-1} (I d/dx - \tau' B) U|_\Gamma + BU|_\Gamma \\
&= \{AD^{-1}d/dx - \tau' AD^{-1}B + B\} U|_\Gamma \\
&= \{AD^{-1}d/dx + (I - \tau' A(I + \tau' A)^{-1}) B\} U|_\Gamma
\end{aligned}$$

Here we have noticed that the matrices  $\tau' A$  and  $(I + \tau' A)^{-1}$  commute and hence

$$I - \tau' A(I + \tau' A)^{-1} = (I + \tau' A)^{-1} = D^{-1}.$$

Since  $A$  and  $D$  also commute,

$$(\partial_t U)|_\Gamma = D^{-1} (A d/dx + B) U|_\Gamma = D^{-1} \Delta U_0$$

and thus for the first order Taylor coefficient we finally have

$$(\partial_t U)|_\Gamma = D^{-1} \Delta (U|_\Gamma) = D^{-1} \Delta U_0. \quad (30)$$

Our computation of higher order Taylor coefficients will be based on the following observation. Since  $\partial_t$  and  $A(x)$  commute,  $\partial_t U$  is also a solution to  $\partial_t U = \Delta U$ , i.e.

$$\partial_t (\partial_t U) = \Delta (\partial_t U),$$

and on the curve

$$(\partial_t U)|_\Gamma = D^{-1} \Delta U_0 \equiv U_1 \quad (\text{by (30)}).$$

Thus, if  $U$  is the solution originated from  $U_0$  then  $\partial_t U$  is the solution originated from the IC  $U_1 = D^{-1} \Delta U_0$ . By induction one concludes that  $\partial_t^k U$  is the solution originated from  $U_k = D^{-1} \Delta U_{k-1}$ ,  $k = 2, 3, 4, \dots$

Therefore, we get the following nice formula

$$\left( \partial_t^k U \right)|_\Gamma = (D^{-1} \Delta)^k U_0, \quad k = 0, 1, 2, \dots$$

Substituting this into (28) we finally arrive at

$$U_n(x) = \sum_{k=0}^n \frac{1}{k!} (-\tau(x))^k (D^{-1} \Delta)^k U_0(x), \quad (31)$$

where, if we recall,

$$D = I + \tau'(x)A(x) \quad (32)$$

$$\Delta = A(x) d/dx + B(x). \quad (33)$$

Note that in (33) we have the full derivative as in (31) we have only one variable. We indicate that  $U_0(x)$ , the original IC on the curve, is only the zero order approximation of our  $U_n(x)$ , which suggests that  $U_n(x)$  is rather a projection than an approximation.

Explicit expanding  $(D^{-1}\Delta)^k$  in (31) is extremely unwieldy but numerical implementation of (31) does not cause any problems. Similar to Nicolsky et al. (2018), where we have a bit more complicated formula for  $U_n(x)$ , the following recursion formula for (31) could be obtained:

$$U_n = U_{n-1} - \frac{1}{n}\tau D^{-1}A(U'_{n-1} - U'_{n-2}) + \frac{n-1}{n}\tau' D^{-1}A(U_{n-1} - U_{n-2}) - \frac{1}{n}\tau D^{-1}B(U_{n-1} - U_{n-2}).$$

It follows from (31) that the map  $U_0 \rightarrow U_n$  is linear and well-defined as long as the matrix  $D$  is non-singular, i.e.

$$\det(I + \tau'(x)A(x)) \neq 0, \quad (34)$$

and the entries of  $A$ ,  $B$ , and  $\tau'$  are at least  $n$  times continuously differentiable. We investigate these conditions for the power-shaped bays later in Subsection 4.2.

## 2.2 Boundary value problem

The considerations of the previous subsection can be easily adjusted to the BVP. Let  $U$  be a column of dependent variables specified on a curve  $\Gamma = \{(f(t), t) | t \geq 0\}$ , i.e.

$$U|_{\Gamma} = U_0. \quad (35)$$

Condition (35) can be viewed as a boundary condition at a variable point  $x_b = f(t)$ . Such a situation occurs when we study the SWE on a finite interval  $x_s \leq x \leq l = \text{const}$  and map it to the hodograph plane using the CG transform. While the shoreline  $x_s$  becomes fixed in the hodograph plane, the other end becomes a floating point. As above we show that given accuracy  $\varepsilon$ , we can find a standard boundary condition at some point  $x_0$  such that the IBVP problem,

$$\begin{cases} \partial_t U = A\partial_x U + BU \\ U|_{x=x_0} = \widetilde{U}_0(t) \\ \text{some IC} \end{cases} \quad (36)$$

has the solution  $\widetilde{U}_0(x, t)$  different from the solution  $U(x, t)$  to (23)-(35) by not more than  $\varepsilon$ .

Let  $x_0$  be a fixed point, e.g. we can take  $x_0 = f(0)$ . Then by Taylor's formula we have

$$U(x_0, t) = \sum_{k=0}^n \frac{1}{k!} \partial_x^k U(x, t)(x_0 - x)^k + E_n, \quad (37)$$

where  $x$  is taken so that  $(x, t) \in \Gamma$  and  $E_n$  is the error term. Consequently, if we are able to find  $\partial_x^k U(x, t)$  and demonstrate that  $|E_n| < \varepsilon$  then,

$$\widetilde{U}_0(t) = \sum_{k=0}^n \frac{1}{k!} \partial_x^k U(x, t) (x_0 - x)^k$$

will be the desired BC in (36). Thus the problem boils down again to finding  $\partial_x^k U|_\Gamma$  in terms of  $U_0$  and  $\Gamma$ . Below  $U|_\Gamma = U(f(t), t)$  and of course  $\frac{d}{dt}U|_\Gamma \neq (\partial_t U)|_\Gamma$ . Differentiating  $U|_\Gamma = U_0(t)$  by the chain rule

$$\begin{aligned} \frac{d}{dt}(U|_\Gamma) &= \partial_x U|_\Gamma \cdot x'(t) + \partial_t U|_\Gamma \\ &= \partial_x U|_\Gamma \cdot f' + (A\partial_x U)|_\Gamma + (BU)|_\Gamma \\ &= (A|_\Gamma + f'I)\partial_x U|_\Gamma + B|_\Gamma(U|_\Gamma) \end{aligned}$$

we find

$$\partial_x U|_\Gamma = (A|_\Gamma + f'I)^{-1} \left( \frac{d}{dt}(U|_\Gamma) - B|_\Gamma(U|_\Gamma) \right).$$

Thus, recalling that  $U|_\Gamma = U_0$ , we have

$$\partial_x U|_\Gamma = D^{-1}(U'_0 - B|_\Gamma U_0) \tag{38}$$

where  $D \equiv A|_\Gamma + f'I$ . At this point we make a simplifying assumption pertinent to our specific equation below. Suppose that  $A' = \text{const}$  and  $B' = 0$ . In such a case a nice formula can be derived. Indeed, differentiating (23) with respect to  $x$ , we have

$$\partial_t(\partial_x U) = A\partial_x(\partial_x U) + (dA/dx + B)\partial_x U.$$

Thus, if  $U$  solves (23)-(35) then  $\partial_x U$  solves

$$\begin{aligned} \partial_t U &= A\partial_x U + (B + A')U \\ U|_\Gamma &= U_1 \end{aligned}, \tag{39}$$

where  $U_1 = D^{-1}(U'_0 - BU_0)$ . One can now see that the new problem (39) is different from (23)-(35) by the substitutions

$$B \longrightarrow B_1 = B + A', \quad U_0 \longrightarrow U_1. \tag{40}$$

This means that (38) applies with updated data  $B_1$  and  $U_1$ :

$$\begin{aligned}\partial_x^2 U|_\Gamma &= D^{-1}(U_1' - B_1 U_1) \\ &= D^{-1}\left(\frac{d}{dt} - B_1\right)U_1 \\ &= D^{-1}\left(\frac{d}{dt} - B_1\right)D^{-1}\left(\frac{d}{dt} - B\right)U_0\end{aligned}$$

and the following pattern emerges

$$\partial_x^k U|_\Gamma = D^{-1}\left(\frac{d}{dt} - B_{k-1}\right)D^{-1}\left(\frac{d}{dt} - B_{k-2}\right)\dots D^{-1}\left(\frac{d}{dt} - B_0\right)U_0, \quad (41)$$

where  $B_j = B_{j-1} + A'$ ,  $j = 1, 2, \dots, k$  with  $B_0 = B$ .

Thus problem (36) is completely solved. Indeed let  $A, B$  be subject to  $A' = \text{const}$ ,  $B' = 0$ . By taking  $n$  large enough such that the solution  $U$  to

$$\begin{cases} \partial_t U = A\partial_x U + BU \\ U|_\Gamma = U_0 \\ \text{some IC} \end{cases}, \quad \Gamma = \{(f(t), t)\}$$

differs by not more than  $\varepsilon$  from  $\tilde{U}$  which solves the standard IBVP

$$\begin{cases} \partial_t U = A\partial_x U + BU \\ U|_{x=L} = \tilde{U}_0(t) \\ \text{some IC} \end{cases},$$

where

$$\tilde{U}_0(t) = \sum_{k=0}^n \frac{(x_0 - f(t))^k}{k!} \partial_x^k U(x, t) \Big|_\Gamma, \quad (42)$$

and  $\partial_x^k U|_\Gamma$  is given by (41). The choice of  $x_0$  is at our disposal. It can be chosen to be compatible with the IC.

We conclude this section by noting that the Carrier-Greenspan transform reduces the SWE to a linear wave equation on a variable interval. Our method then makes this interval fixed and the transformed equation can then be effectively solved by any applicable method.

### 3 Method of Data Projection for the SWE

In this section we apply our method to the study of the SWE (1) for inclined bays with arbitrary IC. The application of the data projection method for the arbitrary BC will be discussed in the



following section in the context of power-shaped inclined bays, because of certain restrictions on the matrices. As we have seen, projections of IC and BC do not affect the equation itself and therefore we can do IC and BC separately, which is of course technically much easier. After that one can merely put them together by superposition.

### 3.1 Conditions on the IC for the data projection method

With all formulas prepared in the previous section we only need to show that our machinery to solve (7) runs smoothly unless the gradient catastrophe (wave breaking) occurs. The latter happens when invertibility of the CG transform (10b) or its inverse fails (see Rybkin et al., 2014), i.e. when

$$\det \frac{\partial(\sigma, \tau)}{\partial(x, t)} = 0 \text{ or } \det \frac{\partial(x, t)}{\partial(\sigma, \tau)} = 0. \quad (43)$$

The Jacobian in (43) on the left has a nice formula

$$\begin{aligned} \det \frac{\partial(\sigma, \tau)}{\partial(x, t)} &= \det \begin{pmatrix} \partial_x \sigma & \partial_x \tau \\ \partial_t \sigma & \partial_t \tau \end{pmatrix} = \partial_x \sigma \partial_t \tau - \partial_t \sigma \partial_x \tau \\ &= \det \begin{pmatrix} 1 + \partial_x \eta & -\partial_x u \\ \partial_t \eta & 1 - \partial_t u \end{pmatrix} \quad (\text{by (10b)}) \\ &= (1 + \partial_x \eta)^2 - (c(x + \eta) \partial_x u)^2 \quad (\text{by (7)}) \end{aligned}$$

Hence, at  $t = 0$

$$\begin{aligned} \det \frac{\partial(\sigma, \tau)}{\partial(x, t)} \Big|_{t=0} &= (1 + \eta'_0)^2 - (c(x + \eta_0) u'_0)^2 \quad (\text{in } x \text{ variable}) \\ &= (1 + \eta'_{0|\gamma(\sigma)})^2 - (c(\sigma) u'_{0|\gamma(\sigma)})^2 \quad (\text{in } \sigma \text{ variable}). \end{aligned}$$

Consequently, the condition for the CG transform invertibility reads (recall  $\gamma(\sigma)$  is the solution to  $\sigma = x + \eta_0(x)$ )

$$\left( (1 + \partial_x \eta)^2 - c^2(x + \eta) (\partial_x u)^2 \right)^{\pm 1} \neq 0 \quad (\text{for all } (x, t)), \quad (44)$$

$$\left( (1 + \eta'_0)^2 - (c(x + \eta_0) u'_0)^2 \right)^{\pm 1} \neq 0 \quad (\text{for } t = 0), \quad (45)$$

$$\left( (1 + \eta'_{0|\gamma(\sigma)})^2 - (c(\sigma) u'_{0|\gamma(\sigma)})^2 \right)^{\pm 1} \neq 0 \quad (\text{for all } \sigma \geq 0). \quad (46)$$

Recall that (7) in matrix form in  $(\sigma, \tau)$  is

$$\left\{ \begin{array}{l} \partial_\tau \begin{pmatrix} \varphi \\ \psi \end{pmatrix} + \begin{pmatrix} 0 & 1 \\ c^2(\sigma) & 0 \end{pmatrix} \partial_\sigma \begin{pmatrix} \varphi \\ \psi \end{pmatrix} + \begin{pmatrix} 0 & 0 \\ 1 & 0 \end{pmatrix} \begin{pmatrix} \varphi \\ \psi \end{pmatrix} = 0 \\ \begin{pmatrix} \varphi \\ \psi \end{pmatrix} \Big|_\Gamma = \begin{pmatrix} u_0 \\ \eta_0 + u_0^2/2 \end{pmatrix} \Big|_{\gamma(\sigma)} \end{array} \right. . \quad (47)$$

It follows from the previous section that (47) can be solved by our method of data projection if the condition (34) holds. Rewriting (34) for our specific (47) yields

$$\begin{aligned} \det D &= \det \begin{pmatrix} 1 & (u_0|_{\gamma(\sigma)})' \\ c^2(\sigma) (u_0|_{\gamma(\sigma)})' & 1 \end{pmatrix} = 1 - [c(\sigma) (u_0|_{\gamma(\sigma)})']^2 \\ &= 1 - \left[ c(\sigma) \frac{u_0'|_{\gamma(\sigma)}}{1 + \eta_0'|_{\gamma(\sigma)}} \right]^2 = \frac{(1 + \eta_0'|_{\gamma(\sigma)})^2 - (c(\sigma) u_0'|_{\gamma(\sigma)})^2}{(1 + \eta_0'|_{\gamma(\sigma)})^2} \\ &= (1 + \eta_0'|_{\gamma(\sigma)})^{-2} \det \frac{\partial(\sigma, \tau)}{\partial(x, t)} \Big|_{t=0} . \end{aligned} \quad (48)$$

Here we have used

$$(u_0|_{\gamma(\sigma)})' = \frac{u_0'|_{\gamma(\sigma)}}{1 + \eta_0'|_{\gamma(\sigma)}} ,$$

which follows merely from the chain rule  $(u_0|_{\gamma(\sigma)})' = u_0'|_{\gamma(\sigma)} \gamma'(\sigma)$  and  $\gamma'(\sigma) = (1 + \eta_0'|_{\gamma(\sigma)})^{-1}$ .

It immediately follows from (48) that if the Jacobi matrix  $\frac{\partial(\sigma, \tau)}{\partial(x, t)} \Big|_{t=0}$  is nonsingular then so is  $D$ . Thus the condition (46) is sufficient for  $D$  to be nonsingular.

### 3.2 Algorithm of solving SWE with arbitrary IC

For the reader's convenience we summarized here our main result putting together all related formulas in one place.

Consider the IVP (7) (i.e. the BC are replaced with a natural condition that  $\eta$  and  $u$  are both bounded) with non-breaking IC (i.e. subject to (45)). Perform the generalized CG transform

$$\begin{aligned} \varphi(\sigma, \tau) &= u(x, t), & \psi(\sigma, \tau) &= \eta(x, t) + u^2(x, t)/2, \\ \sigma &= x + \eta(x, t), & \tau &= t - u(x, t), \end{aligned}$$

which reduces (7) to the linear IVP (but with IC on a curve)

$$\left\{ \begin{array}{l} \partial_\tau \psi + c^2(\sigma) \partial_\sigma \varphi + \varphi = 0 \\ \partial_\tau \varphi + \partial_\sigma \psi = 0 \\ \varphi(\sigma, -\varphi_0(\sigma)) = \varphi_0(\sigma) \\ \psi(\sigma, -\varphi_0(\sigma)) = \psi_0(\sigma) \end{array} \right. , \quad (49)$$

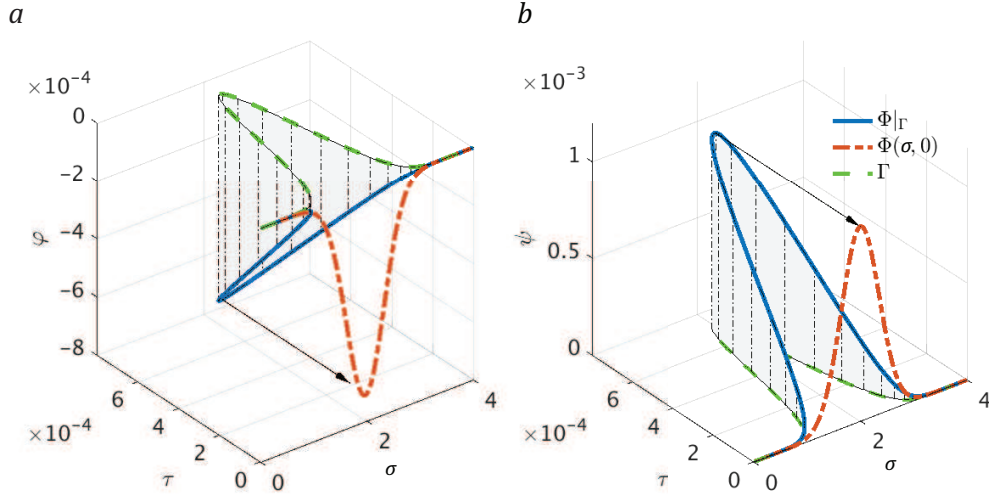


Figure 2: Projection of components  $\Phi|_{\Gamma} = (\varphi, \psi)$  onto the plane  $\tau = 0$  for the initial disturbance with the non-zero water velocity.

where  $\gamma(\sigma)$  is the inverse function of  $\sigma = x + \eta_0(x)$  and

$$\varphi_0(\sigma) = u_0(\gamma(\sigma)), \quad \psi_0(\sigma) = \eta_0(\gamma(\sigma)) + \varphi_0^2(\sigma)/2.$$

Given accuracy  $\varepsilon$  we replace (49) with the standard IVP

$$\begin{cases} \partial_{\tau}\psi + c^2(\sigma)\partial_{\sigma}\varphi + \varphi = 0 \\ \partial_{\tau}\varphi + \partial_{\sigma}\psi = 0 \\ \varphi(\sigma, 0) = \varphi_n(\sigma) \\ \psi(\sigma, 0) = \psi_n(\sigma) \end{cases}, \quad (50)$$

where

$$\begin{pmatrix} \varphi_n(\sigma) \\ \psi_n(\sigma) \end{pmatrix} = \begin{pmatrix} \varphi_0(\sigma) \\ \psi_0(\sigma) \end{pmatrix} + \sum_{k=1}^n \frac{\varphi_0^k(\sigma)}{k!} (D^{-1}\Delta)^k \begin{pmatrix} \varphi_0(\sigma) \\ \psi_0(\sigma) \end{pmatrix}, \quad (51)$$

$$D = \begin{pmatrix} 1 & \varphi_0'(\sigma) \\ c^2(\sigma)\varphi_0'(\sigma) & 1 \end{pmatrix}, \quad \Delta = - \begin{pmatrix} 0 & 1 \\ c^2(\sigma) & 0 \end{pmatrix} \frac{d}{d\sigma} - \begin{pmatrix} 0 & 0 \\ 1 & 0 \end{pmatrix},$$

and  $n$  is chosen so that<sup>3</sup>

$$\max_{\sigma \geq 0} \left\| \frac{\varphi_0^{n+1}(\sigma)}{(n+1)!} (D^{-1}\Delta)^{n+1} \begin{pmatrix} \varphi_0(\sigma) \\ \psi_0(\sigma) \end{pmatrix} \right\| < \varepsilon.$$

<sup>3</sup> $\|\cdot\|$  stands for the Euclidian norm.

Solve (50) analytically or numerically for  $(\varphi(\sigma, \tau), \psi(\sigma, \tau))$ . This  $(\varphi, \psi)$  also solves (49) up to error  $O(\varepsilon)$ . Performing the inverse CG transform

$$\begin{aligned} u(x, t) &= \varphi(\sigma, \tau), & \eta(x, t) &= \psi(\sigma, \tau) - u^2(x, t)/2, \\ x &= \sigma - \eta(x, t), & t &= \tau + u(x, t), \end{aligned}$$

gives us the solution  $(\eta(x, t), u(x, t))$  of (7) up to error  $O(\varepsilon)$ . This solution remains valid as long as the non-breaking condition (44) is satisfied. To obtain the solution for given values of  $(x, t)$ , Newton-Raphson iterations could be employed (Synolakis, 1987; Kanoglu, 2004). An example of data projection is depicted in figure 2.

If the wave reaches a gradient catastrophe (i.e. it breaks) at some point then our SWE (1) is no longer valid and some other approximations of the Navier-Stokes equations should be used (e.g. Johnson, 1997).

## 4 Example of power-shaped bays

In this section we apply the algorithm from Subsection 3.2 to the case when  $f(y) \sim |y|^m$ ,  $0 < m \leq \infty$  (called a power-shaped bay). We then have explicitly  $c(\sigma) = \omega\sqrt{\sigma}$ , where  $\omega = \sqrt{m/(m+1)}$ .

### 4.1 Solution by data projection techniques

In this subsection we consider the case of IC. The linear system (50) then reads

$$\left\{ \begin{array}{l} \partial_\tau \psi + \omega^2 \sigma \partial_\sigma \varphi + \varphi = 0 \\ \partial_\tau \varphi + \partial_\sigma \psi = 0 \\ \varphi(\sigma, 0) = \varphi_n(\sigma) \\ \psi(\sigma, 0) = \psi_n(\sigma) \\ |\varphi(0, \tau)|, |\psi(0, \tau)| < \infty \\ \varphi(\infty, \tau), \psi(\infty, \tau) = 0 \end{array} \right. , \quad (52)$$

where we have merely supplemented the IVP with physically motivated BC.

Compute  $\varphi_n, \psi_n$  in (52) by (51) with  $n$  sufficiently large to provide a negligible error. The new equivalent problem admits an explicit solution in terms of Bessel functions. One can merely do it by the Hankel transform. Instead, we however use the explicit formulas readily available from our Anderson et al. (2017). For the reader's convenience we outline the derivation from Anderson et al. (2017). Reduce the system of PDEs in (52) to the single linear PDE

$$\partial_\tau^2 \psi = \omega^2 \sigma \partial_\sigma^2 \psi + \partial_\sigma \psi. \quad (53)$$

Note that the differential operation on the right hand side of (53) has a regular singular point at  $\sigma = 0$ . This means that (53) has a bounded and an unbounded solution at  $\sigma = 0$ . The latter one is discarded by the boundedness condition at  $\sigma = 0$ . By the standard Hankel transform techniques then for the general solution to (53) we have

$$\psi(\sigma, \tau) = \sigma^{-\frac{1}{2m}} \int_0^\infty \{a(k) \cos(\omega k \tau) + b(k) \sin(\omega k \tau)\} J_{1/m}(2k\sqrt{\sigma}) dk, \quad (54)$$

where  $J_\nu$  is the Bessel function of the first kind of order  $\nu$  and  $a(k)$  and  $b(k)$  are arbitrary functions determined by IC. It follows then from (52) and (54) that

$$\varphi(\sigma, \tau) = \frac{1}{\omega} \sigma^{-\frac{1}{2m} - \frac{1}{2}} \int_0^\infty \{a(k) \sin(\omega k \tau) - b(k) \cos(\omega k \tau)\} J_{1/m+1}(2k\sqrt{\sigma}) dk. \quad (55)$$

We note that the apparent singularities at  $\sigma = 0$  in (54) and (55) are actually removable due to asymptotic properties of the Bessel function of the first kind around 0.

The functions  $a$  and  $b$  can now be found from the IC by applying the inverse Hankel transform to (54) and (55):

$$a(k) = 2k \int_0^\infty \psi_n(s) s^{\frac{1}{2m}} J_{\frac{1}{m}}(2k\sqrt{s}) ds, \quad (56a)$$

$$b(k) = -2\omega k \int_0^\infty \varphi_n(s) s^{\frac{1}{2m} + \frac{1}{2}} J_{\frac{1}{m}+1}(2k\sqrt{s}) ds \quad (56b)$$

where  $\psi_n(s), \varphi_n(s)$  are computed by (51). Thus  $\psi$  and  $\varphi$  are completely determined and (52) is explicitly solved.

In particular, for waves with zero initial velocity (i.e.  $u_0 = 0$  and hence  $\varphi_0 = 0$ )  $b(k) = 0$  and

$$a(k) = 2k \int_{x_0}^\infty [x + \eta_0(x)]^{\frac{1}{2m}} J_{1/m}\left(2k\sqrt{x + \eta_0(x)}\right) [1 + \eta_0'(x)] \eta_0(x) dx, \quad (57)$$

where we have used a simple change of variables to return back to the physical space, and  $x_0$  is the maximum run-up (i.e.  $x_0 + \eta_0(x_0) = 0$ ).

## 4.2 Finite power-shaped bay

Here we consider a power-shaped bay  $f(y) \sim |y|^m$ ,  $0 < m \leq \infty$  of finite length  $l$  and set up some boundary conditions at  $l$ , e.g. see (Harris et al., 2016)

$$\eta(l, t) = \eta_b(t), \quad u(l, t) = u_b(t).$$

Since  $B$  is a constant matrix and

$$A' = \frac{d}{d\sigma} \begin{pmatrix} 0 & 1 \\ \omega^2 \sigma & 0 \end{pmatrix} = \begin{pmatrix} 0 & 0 \\ \omega^2 & 0 \end{pmatrix}$$

is also a constant matrix, the results of Subsection 2.2 apply. Recall that the constant  $\omega = \sqrt{m/(m+1)}$ . For the curve we have

$$\Gamma_b = \{(\sigma_b(\tau), \tau) \mid \gamma_b(\tau) \geq 0\},$$

where  $\gamma_b(\tau)$  is the inverse function of  $\tau = t - u_b(t)$  and

$$\sigma_b(\tau) = l + \eta_b|_{\gamma_b(\tau)}.$$

Eq. (41) reads

$$\partial_\sigma^k \Phi|_{\Gamma_b} = D^{-1} \left( \frac{d}{d\tau} + B_{k-1} \right) D^{-1} \left( \frac{d}{d\tau} + B_{k-2} \right) \dots D^{-1} \left( \frac{d}{d\tau} + B_0 \right) \Psi_0,$$

where

$$D \equiv \begin{pmatrix} \sigma'_b(\tau) & -1 \\ -\omega^2 \sigma_b(\tau) & \sigma'_b(\tau) \end{pmatrix}, \quad B_k = \begin{pmatrix} 0 & 0 \\ 1 + k\omega^2 & 0 \end{pmatrix}.$$

Eq. (42) for our case now yields

$$\tilde{\Psi}_0(\tau) = \sum_{k=0}^n \frac{(\sigma_0 - \sigma_b(\tau))^k}{k!} \partial_\sigma^k \Phi|_{\Gamma_b}.$$

Thus the problem with a floating boundary condition is reduced to a fixed one

$$\left\{ \begin{array}{l} \partial_\tau \psi + \omega^2 \sigma \partial_\sigma \varphi + \varphi = 0 \\ \partial_\tau \varphi + \partial_\sigma \psi = 0 \\ \varphi(\sigma, 0) = \varphi_n(\sigma) \\ \psi(\sigma, 0) = \psi_n(\sigma) \\ \varphi(\sigma_0, \tau) = \tilde{\varphi}_b(\tau) \\ \psi(\sigma_0, \tau) = \tilde{\psi}_b(\tau) \end{array} \right. \quad (58)$$

Here,  $\tilde{\varphi}_b(\tau)$ ,  $\tilde{\psi}_b(\tau)$  are components of the vector  $\tilde{\Psi}_0(\tau)$ . The value of  $\sigma_0$  is chosen to be compatible with the IC, or  $\sigma_0 = l + \eta_0(l, 0)$ .

Note that an arbitrary boundary condition at  $l$  need not produce a bounded solution to (58), i.e. we may have an infinite run-up (the energy will of course be finite). The physical relevance of such solutions is debatable but they can be avoided by imposing a compatibility condition for  $(\eta_b, u_b)$ .

Such compatibility conditions are dictated by the underlying physics (e.g. Antuono and Brocchini, 2007, 2010).

Assuming that  $\eta_b$  and  $u_b$  are compatible, we can then handle

$$\left\{ \begin{array}{l} \partial_\tau^2 \psi = \omega^2 \sigma \partial_\sigma^2 \psi + \partial_\sigma \psi \\ \psi(\sigma, 0) = \psi_n(\sigma) \\ \psi_\tau(\sigma, 0) = -\omega^2 \sigma \partial_\sigma \varphi_n(\sigma) - \varphi_n(\sigma) \\ \psi(\sigma_0, \tau) = \tilde{\psi}_b(\tau) \\ |\psi(0, \tau)| < \infty \end{array} \right. \quad (59)$$

by a Bessel-Fourier expansion as follows.

By introducing the change of variables  $\zeta^2 = \sigma/\sigma_0$  and  $\psi(\sigma, \tau) = \zeta^{-\gamma} \theta(\zeta, \tau) + \tilde{\psi}_b(\tau)$ , where  $\gamma = 1/m$ , the wave equation is obtained

$$\partial_\tau^2 \theta = k^2 \left( \partial_\zeta^2 \theta + \frac{1}{\zeta} \partial_\zeta \theta - \frac{\gamma^2}{\zeta^2} \theta \right) - \zeta^\gamma \tilde{\psi}_b''(\tau), \quad (60)$$

which admits a solution in terms of the Bessel functions  $J_\gamma$  of order  $\gamma$ . Here, the prime denotes a derivative with respect to  $\tau$ ,  $k^2 = \omega^2/4\sigma_0$ , and  $\zeta \in [0, 1]$ . The boundary condition at  $\sigma = \sigma_0$  is transformed to  $\theta(1, \tau) = 0$ . Next, the Fourier-Bessel decomposition is employed so that

$$\theta(\zeta, \tau) = \sum_{n=1}^{\infty} c_n(\tau) J_\gamma(j_n \zeta). \quad (61)$$

To solve for the coefficients, we substitute (61) into (60) and use an orthogonality property of Bessel functions to obtain a set of ordinary differential equations for each coefficient  $c_n$ :

$$c_n''(\tau) + (j_n k)^2 c_n(\tau) = -\frac{2}{J_{\gamma+1}^2(j_n)} \tilde{\psi}_b''(\tau) \int_0^1 \zeta^{1+\gamma} J_\gamma(j_n \zeta) d\zeta. \quad (62)$$

The initial conditions in (59) could be cast to yield the initial conditions for  $c_n$  such that

$$\begin{aligned} c_n(0) &= \frac{2}{J_{\gamma+1}^2(j_n)} \int_0^1 \zeta^{1+\gamma} J_\gamma(j_n \zeta) \left[ \psi_n(\sigma_0 \zeta^2) - \tilde{\psi}_b(0) \right] d\zeta, \\ c_n'(0) &= -\frac{2}{J_{\gamma+1}^2(j_n)} \int_0^1 \zeta^{1+\gamma} J_\gamma(j_n \zeta) \left[ \frac{1}{2} \omega^2 \zeta \partial_\zeta \varphi_n(\sigma_0 \zeta^2) + \varphi_n(\sigma_0 \zeta^2) + \tilde{\psi}_b'(0) \right] d\zeta. \end{aligned}$$

Finally, we express  $\psi$  and  $\phi$  in terms of variables  $(\sigma, \tau)$  as

$$\psi(\sigma, \tau) = \left( \frac{\sigma_0}{\sigma} \right)^{\frac{1}{2m}} \sum_{n=1}^{\infty} c_n(\tau) J_{\frac{1}{m}}(j_n \sqrt{\sigma/\sigma_0}) + \tilde{\psi}_b(\tau), \quad (63)$$

$$\varphi(\sigma, \tau) = \frac{1}{2\sigma_0} \left( \frac{\sigma_0}{\sigma} \right)^{\frac{1}{2m} + \frac{1}{2}} \sum_{n=1}^{\infty} j_n d_n(\tau) J_{\frac{1}{m}+1}(j_n \sqrt{\sigma/\sigma_0}), \quad (64)$$

where,

$$d_n(\tau) = \int_0^\tau c_n(\lambda) d\lambda.$$

We calculate runup and rundown of the Gaussian wave in a V-shaped bay ( $\omega = 1/\sqrt{2}$ ) using equations (63)-(64) in Subsection 4.2.

### 4.3 Comparison to previous results

As we have mentioned in the introduction, the problem of adjusting the CG transform techniques to an arbitrary nonzero initial velocity has been approached by many authors. We will not discuss the complete history of the problem and by the same token will not give an attempt to review the extensive literature. Instead, we concentrate only on the most important contributions where the interested reader can find further references.

The first significant result to this effect appeared in Carrier et al. (2003). It was then improved in Kanoglu (2004) and Kanoglu and Synolakis (2006), where the Green's function approach was employed. More specifically, for the plane beach ( $m = \infty$ ) under the assumption that  $\sigma = x$  a certain solution formula was derived. It can be shown (see our (Nicolosky et al., 2018) for the details) that this solution is exact only if  $\varphi'_0(\sigma) = 0$ . However, for near shore waves with large initial velocities such solution may produce some artifacts. If  $\varphi'_0(\sigma) = 0$  then  $D = I$  and (51) simplifies to read

$$\begin{aligned} \begin{pmatrix} \varphi_n(\sigma) \\ \psi_n(\sigma) \end{pmatrix} &= \sum_{k=0}^n \frac{\varphi_0^k(\sigma)}{k!} \Delta^k \begin{pmatrix} \varphi_0(\sigma) \\ \eta_0|_{\gamma(\sigma)} + \varphi_0^2(\sigma)/2 \end{pmatrix} \\ &= \begin{pmatrix} \varphi_0(\sigma) \\ \eta_0|_{\gamma(\sigma)} + \varphi_0^2(\sigma)/2 \end{pmatrix} - \varphi_0(\sigma) \begin{pmatrix} 0 \\ (\eta_0|_{\gamma(\sigma)})' + \varphi_0(\sigma) \end{pmatrix} \\ &\quad + \frac{\varphi_0^2(\sigma)}{2} \begin{pmatrix} 0 \\ (1 + c^2(\sigma)) (\eta_0|_{\gamma(\sigma)})' + c^2(\sigma) (\eta_0|_{\gamma(\sigma)})'' \end{pmatrix} + \dots \end{aligned} \quad (65)$$

It is a straightforward (but quite involved) exercise to show that combining (54)-(56b), and (65) yields  $\psi(\sigma, \tau)$  which coincides with the solution in Kanoglu and Synolakis (2006) up to  $O(\varphi'_0(\sigma))$ . However, as numerical simulations in the next subsection show, our scheme runs smoothly without the assumption that  $\varphi'_0(\sigma)$  is small. Incidentally, (65) demonstrates the analytical complexity of our data projection method.

In very interesting papers (Antuono and Brocchini, 2007, 2010) perturbation techniques are used to deal with boundary value problems. However, such techniques could also be adjusted to



the IVP but would require certain smallness of the BC and IC.

The IVP has also been considered in the context of parabolic bays where  $m = 2$ . Didenkulova and Pelinovsky (2011a) derived an exact traveling wave solution of the IVP in parabolic bays for waves with zero initial velocity. In parabolic bays where  $m = 2$ , using the identity  $J_{1/2}(x) = \sqrt{2/(\pi x)} \sin(x)$  along with other trigonometric identities, (54) and (57) reduce (again after quite involved computations) to

$$\begin{aligned} \psi(\sigma, \tau) &= \frac{1}{2\sqrt{\sigma}} \left\{ \Theta \left( \sqrt{\sigma} + \frac{\tau}{\sqrt{6}} \right) + \Theta \left( \sqrt{\sigma} - \frac{\tau}{\sqrt{6}} \right) \theta \left( \sqrt{\sigma} - \frac{\tau}{\sqrt{6}} \right) - \Theta \left( \frac{\tau}{\sqrt{6}} - \sqrt{\sigma} \right) \theta \left( \frac{\tau}{\sqrt{6}} - \sqrt{\sigma} \right) \right\} \end{aligned}$$

where  $\Theta(\zeta) = \zeta \eta_0(\gamma(\zeta))$ ,  $\theta$  is the Heaviside function, and  $\gamma(\sigma)$ , as before, is given implicitly by  $x + \eta_0(x) = \sigma$ . This solution is identical to the one given by Didenkulova and Pelinovsky (2011a) under the change of variables  $\sigma = \sqrt{6}s$ ,  $\lambda = -\tau$ ,  $\varphi = \phi_\sigma/\sigma$  and  $\psi = \phi_\lambda/3$ .

IBVP in the same context have also been treated by many authors, see (e.g. Synolakis, 1987; Kanoglu, 2004; Anderson et al., 2017) and the literature cited therein, where floating points are fixed by assuming a certain negligible difference between  $\sigma$  and  $x$  far away from the shore. Our approach does not require such assumptions.

## 5 Numerical Verification of the data projection method

### 5.1 Verification for the initial value problem

In this subsection, we numerically verify our data projection method for the initial value problem (52) by considering runup of the Gaussian wave

$$\eta_0(x) = ae^{-b(x-x_0)^2}, \tag{66}$$

in a bay of the parabolic shape ( $m = 2$ ). To do that we consider initial condition  $(\eta_0, 0)$  (i.e. with zero initial velocity) and run it by the standard CG to the maximum runup at  $t = t_r$ . While modeling the runup  $\eta(x, t_r)$ , we record  $(\eta(x, t_*), u(x, t_*))$  at some time  $t_* < t_r$ . We then set up a new IVP with IC  $(\eta(x, t_*), u(x, t_*))$  and run it by our method. Both solutions (via the standard CG and the new IVP) are expected to show an excellent agreement for  $t_r \geq t > t_*$ . Results of the comparison are provided below.

In particular, as in (Kanoglu and Synolakis, 2006; Nicolsky et al., 2018) we consider an initial Gaussian wave with  $a = 0.017$ ,  $b = 4.0$  and centered at the distance of  $x_0 = 1.69$  from the shore.

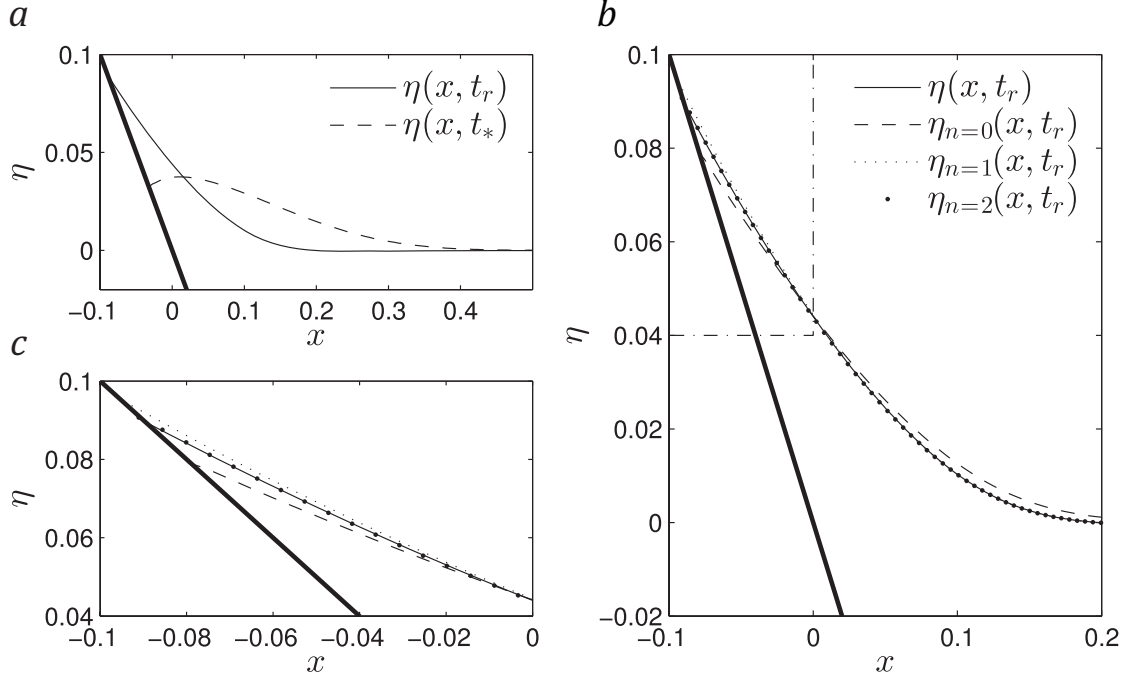


Figure 3: a: profiles of the water level  $\eta$  for the initial condition: a zero-velocity Gaussian wave given by (66) with  $a = 0.017$ ,  $b = 4.0$  and  $x_0 = 1.69$  running up a parabolic bay ( $m = 2$ ). Profile  $\eta(x, t_*)$  is used in the proposed data projection method to solve a non-zero initial velocity problem. b: Comparison of the water level at  $t = t_r$  for various approximations of  $\Phi_n$ . c: Zoomed-in comparison of water level near the shoreline, i.e. within the dashed rectangle is shown in plot b.

In this case, the maximum runup occurs at  $t_r \approx 2.908$ , and we choose  $t_* = 2$ , when the wave is approximately half the way to its maximum runup on the shore (and where of course  $u(x, t_*) \neq 0$ ). Figure 3a displays wave profile at the time of maximum runup  $t_r$  and at the moment  $t_*$ . We launch our method forming the projected IC by (51) with various degrees of approximation  $n = 0, 1, 2$  and apply formulas (54-55) to model the wave propagation until  $t = t_r$ . We note that  $c^2(\sigma) = 2/3\sigma$ . To compute projections of the IC and BC, we use recursive formulae and compute the first order derivatives by the finite differences of the second order accuracy wherever possible.

Comparison of the water level profiles  $\eta(x, t_r)$  and  $\{\eta_{n=k}(x, t_r)\}_{k=0}^2$  at the moment of maximum runup is shown in Figure 3b. Unlike to results by Nicolsky et al. (2018), where the zeroth approximation,  $n = 0$ , was adequate to capture the wave profile at  $t = t_r$ , here the zeroth approximation shows a visible deviation from  $\eta(x, t_r)$  due to a larger initial velocity  $\eta(x, t_*)$  used in the data projection method. Notice that for the high-order approximations,  $n = 1, 2$ , the match between the water profiles at  $t = t_r$  improves and becomes satisfactory. The convergence of approximations,

$\{\eta_{n=k}(x, t_r)\}_{k=0}^2$ , is demonstrated near the tip of the wave; an area within the dashed rectangle in Figure 3b is shown in Figure 3c. One may notice that the zeroth approximation  $\eta_{n=0}(x, t_r)$  undershoots the runup, the first-order approximation  $\eta_{n=1}(x, t_r)$  overshoots and the second order  $\eta_{n=2}(x, t_r)$  almost overlaps  $\eta(x, t_r)$ . Other higher order approximations (not shown for the sake of clarity) provide a nearly exact match to  $\eta(x, t_r)$ . This demonstrates an efficacy of the proposed method to project the solution forward from the given initial conditions.

## 5.2 Verification for the boundary value problem

In this subsection, we numerically verify our data projection method for the boundary value problem (59) by considering runup of the Gaussian wave (66) in a V-shaped bay ( $m = 1$ ,  $c^2(\sigma) = (1/2)\sigma$ ). Similar to the previous numerical experiment, we consider a zero-velocity initial condition  $(\eta_0, 0)$  and run it by the standard CG to compute the maximum runup ( $t = t_r$ ), rundown ( $t = t_d$ ) and the secondary runup  $t = t_s$ . The secondary runup of a Gaussian wave is a feature of the V-shaped bay as it was noted by Garayshin et al. (2016); Nicolsky et al. (2018). Now, while modeling the wave dynamics, we save the time history of  $\eta(x, t)$  and  $u(x, t)$  at some point  $x = x_*$  near the shore (e.g.  $x_* = 0.15$ ) for  $0 \leq t \leq t_s$ . Note that in the previous subsection we recorded the snapshot of the wave dynamics to setup the IVP. Here, we use the saved time history  $(\eta(x_*, t), u(x_*, t))$  to set up a new BVP and run it by our method (assuming in the data projection algorithm that  $l = x_*$ ,  $\eta_b(t) = \eta(x_*, t)$  and  $u_b(t) = u(x_*, t)$ ). Both solutions via the standard CG and the new BVP are again to show an excellent agreement for  $t < t_s$ .

Similar to the previous experiment, we consider an initial Gaussian wave with the same characteristics, but the amplitude is reduced ( $a = 0.017$ ) to have a highest non-breaking wave throughout the simulation. Comparisons between the two solutions at the moments of maximum runup, rundown and the secondary runup are provided in Figure 4. The water level  $\eta_{n=0}$  for the zeroth approximation shows a discrepancy with  $\eta$ . However, results for the next order of approximation, i.e.  $n = 1$ , match the true solution almost exactly at the two run-ups and rundown. Other higher orders rapidly converge and provide nearly exact match.

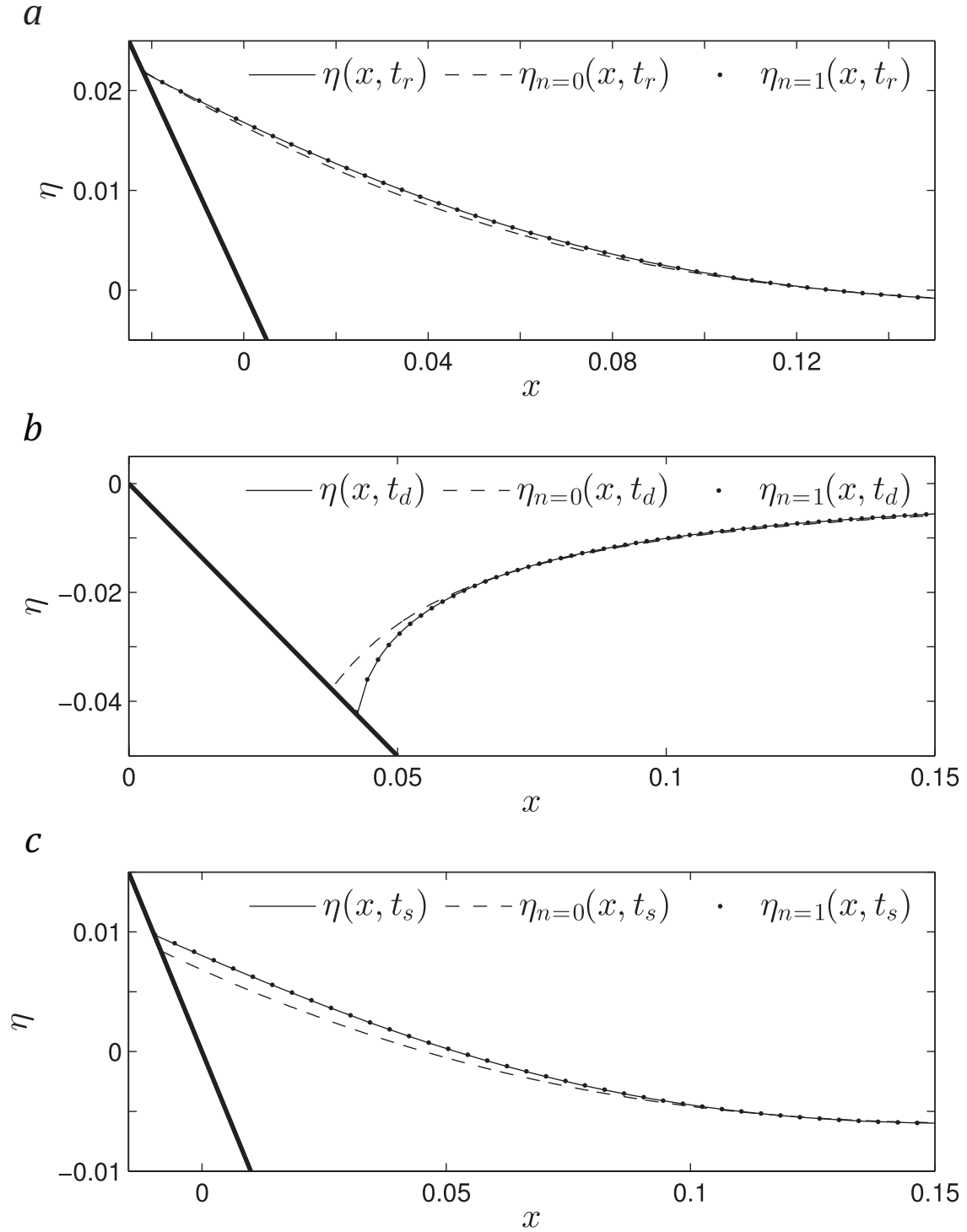


Figure 4: Comparison of the water level profiles  $\eta(x, t)$  and  $\{\eta_{n=k}(x, t)\}_{k=0}^2$  at the moment of (a) maximum runup  $t = t_r$ , (b) rundown  $t = t_d$  and (c) the secondary runup  $t = t_s$  in the V-shaped bay ( $m = 1$ ).

### 5.3 Modeling shore dynamics for the incident N-wave

To illustrate efficacy of the proposed method for BVP (59) we also consider runup of N-shaped waves in the parabolic bay ( $m = 2$ )

$$\eta_0(x) = a_1 e^{-b_1(x-x_1)^2} + a_2 e^{-b_2(x-x_2)^2}. \quad (67)$$

In particular, we consider two leading-depression N-shaped waves with the geometries similar to those in (Carrier et al., 2003). Both waves have zero initial velocities and their profiles are shown in Figure 5. As in the previous subsection, we model the wave dynamics using the standard CG and record the water level as well as the velocity at some point  $x = x_*$  near the shore, e.g. at  $x_* = 0.15$ . The recorded history of  $(\eta(x_*, t), u(x_*, t))$  is then again used to set up a new BVP with  $l = x_*$ ,  $\eta_b(t) = \eta(x_*, t)$  and  $u_b(t) = u(x_*, t)$  to model shoreline dynamics. Figure 6 shows comparison between the shoreline  $\hat{\eta}$  computed with the standard CG and those  $\{\hat{\eta}_{m=k}\}$  obtained from different order approximations, i.e.  $k = 0, 1$ . Notice that even for the zeroth approximation,  $n = 0$ , the match between the shorelines is rather good. However, some discrepancy exists at the maximum runup, the zeroth order overestimates the maximum runup. However, the first order approximation,  $n = 1$ , nearly exactly matches the true solution during the runup and rundown.

### 5.4 Contribution of the wave velocity to runup

We conclude this section with illustrating a physical effect showing how the runup increases when initial velocity is present. When initial velocity is absent the initial wave splits and propagates in both directions from the source region, i.e. towards shore and away from it. It was shown by Didenkulova and Pelinovsky (2011b) that in a flat bottom fjords with the power-shaped cross-section, the wave propagates towards the shore when the initial velocity satisfies

$$u_0(x) = -2\sqrt{(m+1)/m} \left( \sqrt{\eta+h} - \sqrt{h} \right). \quad (68)$$

We use this approximation in the following numerical experiment. As before, we consider the parabolic bay ( $m = 2$ ) and take the same Gaussian wave with  $u_0 = 0$  and with  $u_0$  given by (68) with  $h = x$ . In the former case, the runup occurs  $t_r \approx 2.908$ , whereas in the latter one the runup happens  $t_r \approx 2.928$ . That is, the runup occurs almost at the same time, however, as one can see it in Figure 7, the maximum run-up is almost twice as large for the non-zero initial velocity. This result shows that long waves can be greatly amplified in heads of narrow bays if the initial velocity nonzero.

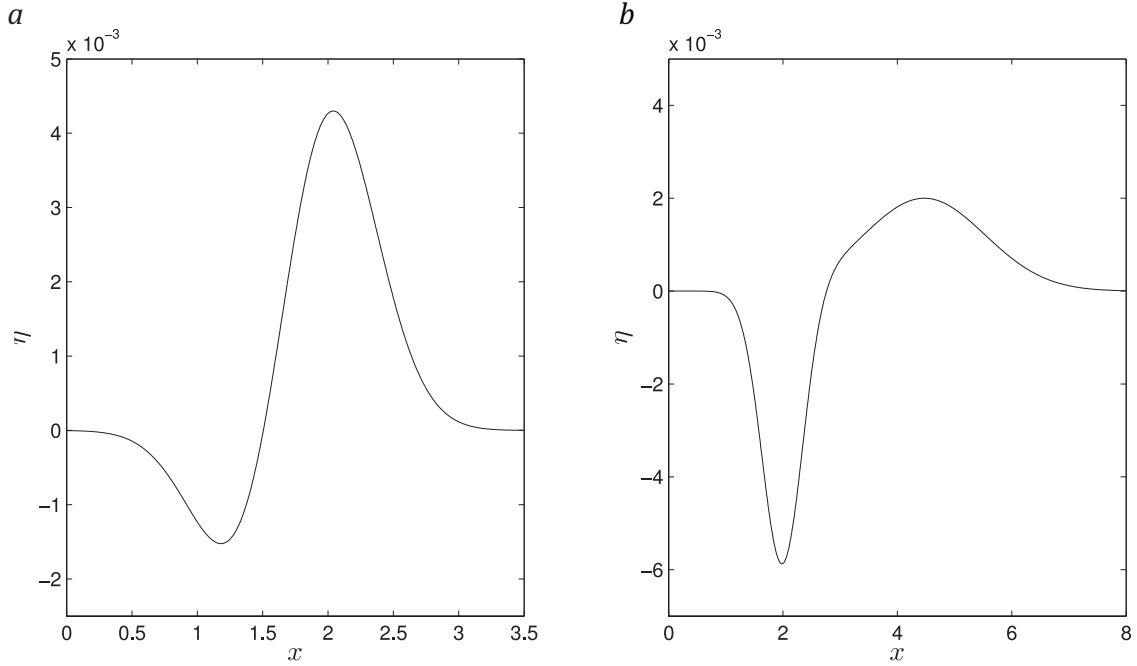


Figure 5: Initial leading-depression N-waves with the geometries similar to Carrier et al. (2003); Kanoglu (2004): (a)  $a_1 = 0.005$ ,  $b_1 = 3.5$ ,  $x_1 = 1.9625$ ,  $a_2 = -0.0025$ ,  $b_2 = 3.5$ , and  $x_2 = 1.4$ . (b)  $a_1 = 0.002$ ,  $b_1 = 0.4444$ ,  $x_1 = 4.4709$ ,  $a_2 = -0.006$ ,  $b_2 = 4.0$ , and  $x_2 = 1.9884$

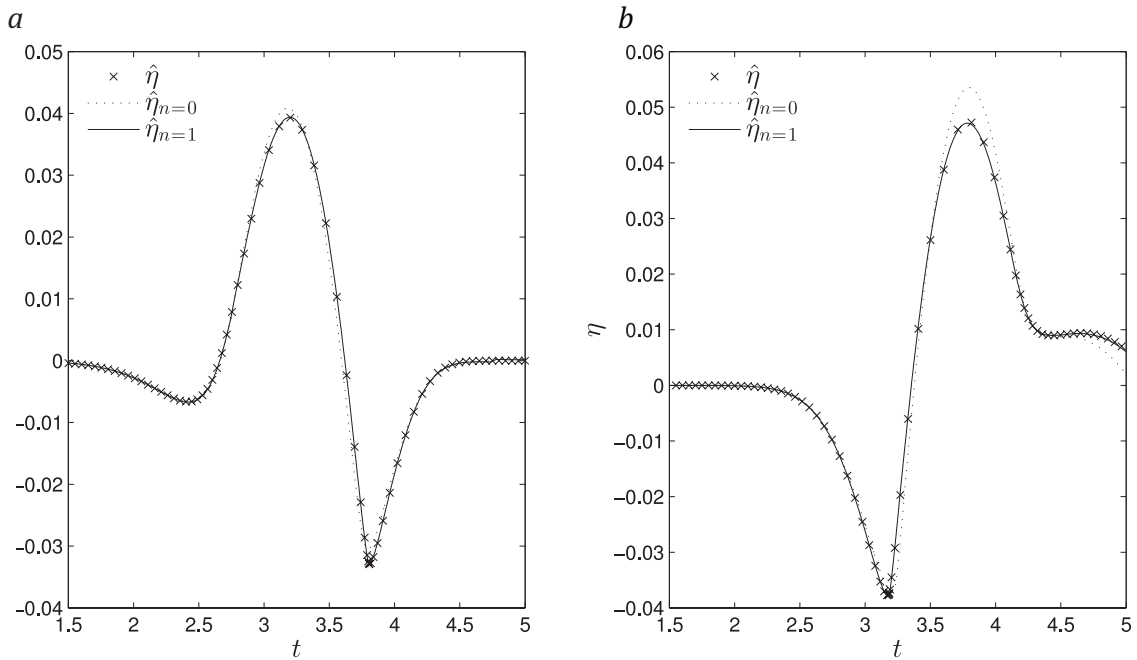


Figure 6: Comparison of the shoreline dynamics  $\hat{\eta}$  for the leading-depression N-waves in the parabolic bay ( $m = 2$ ). Dynamics in (a) and (b) correspond to cases in Figure 5.

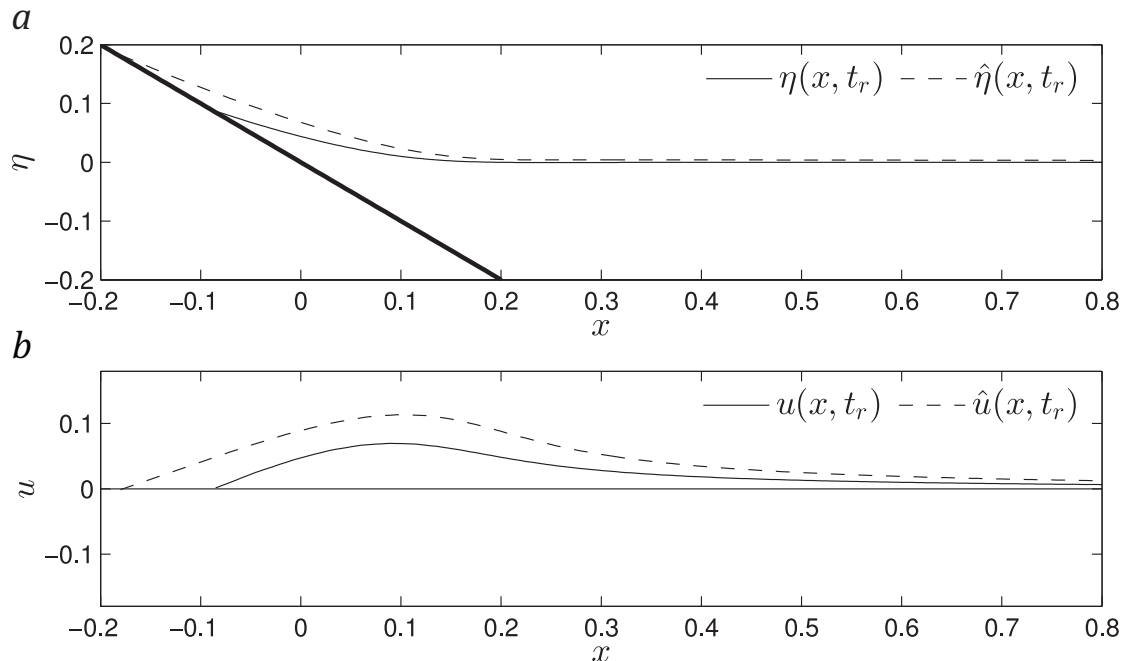


Figure 7: Comparison of the water level (a) and water velocity (b) at the time  $t = t_r$  of maximum runup. Quantities marked with the symbol  $\hat{\cdot}$  are computed in the case when the initial velocity  $u_0(x) = -2\sqrt{(m+1)/m} (\sqrt{\eta+h} - \sqrt{h})$ .

## 6 Conclusions

Our method of data projection completely solves the problem of the effective linearization of the shallow water equation (SWE) for any inclined bay with IC (in arbitrary shaped bays) and BC (only in power-shaped bays) by means of the Carrier-Greenspan (CG) transform. Basing upon Taylor's formula in "reverse", given IC  $\eta(x, 0) = \eta_0(x)$ ,  $u(x, 0) = u_0(x)$  (with  $u_0 \neq 0$ ) for the (7), we find an equivalent IC  $\varphi(\sigma, 0) = \varphi_n(\sigma)$ ,  $\psi(\sigma, 0) = \psi_n(\sigma)$  for the linear SWE (13) in the transformed space  $(\sigma, \tau)$  (hodograph plane). The initial value problem (IVP) (50) can then be easily solved analytically or numerically. Performing the inverse CG transform solves the original IVP for the SWE (7) to any order of accuracy. As is well-known, the main benefits of (in fact, any) linearization are nearly instantaneous computations and explicit analysis uncovering subtle properties of the system under consideration. This method works songlessly for BC as well and hence for IC/BC combined. The BC case though requires more attention than we were able to pay in this paper. In particular, our approach may potentially be very useful in the study of more complicated than inclined bathymetries treated in (Synolakis, 1987, 1991).

Our method, which becomes explicit for U-shaped bays, has potential applications in tsunami wave modeling. Tsunami forecast models are extensively verified against the analytical solutions of the SWEs (Synolakis et al., 2008), primarily for the case of a plane beach. This solution allows further analytical verification of tsunami models, with the extension of the solution to 2-D bathymetries, allowing verification of tsunami models in realistic settings. As local near-shore bathymetry significantly effects the run-up of tsunami waves, and narrow bays can greatly amplify tsunami waves, the verification of tsunami models in narrow bays is critical for protecting coastal communities and infrastructure. Furthermore, 1-D nonlinear shallow water theory has had significant developments in the past few years, specifically in the context of narrow bays. In the realistic setting of Alaskan fjords, 1-D theory has had similar runup predictions to full 2-D tsunami models with significantly less computation time (Harris et al., 2015; Anderson et al., 2017). 1-D theory can even present valid predictions in splitting bays (Raz et al., 2018). With such progress, it is possible for 1-D shallow water theory to be incorporated into global 2-D tsunami inundation models, specifically in narrow bays and fjords. This will reduce computation and forecasting time, potentially saving lives and resources.

Treating initial and boundary conditions for the SWE by means of the CG transform opens new avenues in the analysis of much more realistic runup problems for tsunami waves. In particular, we hope to develop a method of stitching together different shallow water approximations describing different stages of the tsunami wave propagation.

**Acknowledgments:** We would like to thank anonymous referees for careful reading of the manuscript and valuable comments, which have been very helpful in improving the manuscript. Also, we are grateful to Dillon Gillespie for his help with computations of the Bessel-Fourier expansion. Alexei Rybkin acknowledges support from National Science Foundation Grant (NSF) award DMS-1411560 and DMS-1716975. Dmitry Nicolsky acknowledges support from the Geophysical Institute, University of Alaska Fairbanks. Efim Pelinovsky acknowledges support by Laboratory of Dynamical Systems and Applications NRU HSE, by the Ministry of science and higher education of the RF grant ag. 075-15-2019-1931 and by FRBR grant 18-05-80019 and 20-05-00162. Maxwell Buckel was supported by the National Science Foundation Research Experience for Undergraduate program (Grant DMS-1411560).



## References

- Alekseenko, S., Dontsova, M., and Pelinovsky, D. (2017). Global solutions to the shallow water system with a method of an additional argument. *Applicable Analysis*, 69(9):1444–1465.
- Anderson, D., Harris, M., Hartle, H., Nicolsky, D., Pelinovsky, E., Raz, A., and Rybkin, A. (2017). Run-up of long waves in piecewise sloping u-shaped bays. *Journal of Pure and Applied Geophysics*, 174:3185–3207.
- Antuono, M. and Brocchini, M. (2007). The boundary value problem for the nonlinear shallow water equations. *Studies in Applied Mathematics*, 119:73–93.
- Antuono, M. and Brocchini, M. (2010). Solving the nonlinear shallow-water equations in physical space. *Journal of Fluid Mechanics*, 643:207232.
- Carrier, G. and Greenspan, H. (1958). Water waves of finite amplitude on a sloping beach. *J. Fluid Mech.*, 01:97–109.
- Carrier, G., Wu, T., and Yeh, H. (2003). Tsunami run-up and draw-down on a plane beach. *J. Fluid Mech.*, 475:79–99.
- Chugunov, V., Fomin, S., Noland, W., and Sagdiev, B. (2020). Tsunami runup on a sloping beach. *Computational and Mathematical Methods*, 2:e1081.
- Chugunov, V., Fomin, S., and Shankar, R. (2014). Influence of underwater barriers on the distribution of tsunami waves. *Journal of Geophysical Research: Oceans*, 119:7568–7591.
- Craig, W. (2006). Surface water waves and tsunamis. *Journal of Dynamics and Differential Equations*, 18(3):525–549.
- Craig, W. and Groves, M. (1994). Hamiltonian long-wave approximations to the water-wave problem. *Wave Motion*, 19:367–389.
- Craig, W., Guyenne, P., and Kalisch, H. (2004). A new model for large amplitude long internal waves. *Comptes Rendus Mecanique*, 332:525–530.
- Craig, W., Guyenne, P., and Kalisch, H. (2005a). Hamiltonian long wave expansions for free surfaces and interfaces. *Communications on Pure and Applied Mathematics*, 58(12):1587–1641.

- Craig, W., Guyenne, P., Nicholls, D., and Sulem, C. (2005b). Hamiltonian long-wave expansions for water waves over a rough bottom. *Proceedings of the Royal Society of London. Series A*, 461(839-873).
- Craig, W. and Wayne, C. (2007). Mathematical aspects of surface water waves. *Russian Mathematical Surveys*, 62(3):453–473.
- Didenkulova, I. and Pelinovsky, E. (2011a). Non-linear wave evolution and run-up in an inclined channel of a parabolic cross-section. *Physics of Fluids*, 23:086602.
- Didenkulova, I. and Pelinovsky, E. (2011b). Rogue waves in nonlinear hyperbolic systems (shallow-water framework). *Nonlinearity*, 24:R1–18.
- Dobrokhotov, S., Medvedev, S., and Minenkov, D. (2013). On transforms reducing one-dimensional systems of shallow-water to the wave equation with sound speed  $c^2 = x$ . *Mathematical Notes*, 93:704–714.
- Dobrokhotov, S., Nazaikinskii, V., and Tirozzi, B. (2010). Asymptotic solution of the one-dimensional wave equation with localized initial data and with degenerating velocity: I. *Russian Journal of Mathematical Physics*, 17(4):434–450.
- Dobrokhotov, S. and Tirozzi, B. (2010). Localized solutions of one-dimensional non-linear shallow-water equations with velocity  $c = \sqrt{x}$ . *Russian Mathematical Surveys*, 65(1):177–179.
- Garayshin, V., Harris, M., Nicolsky, D., Pelinovsky, E., and Rybkin, A. (2016). An analytical and numerical study of long wave run-up in u-shaped and v-shaped bays. *Applied Mathematics and Computation*, 297:187–197.
- Harris, M., Nicolsky, D., Pelinovsky, E., Pender, J., and Rybkin, A. (2016). Run-up of nonlinear long waves in u-shaped bays of finite length: Analytical theory and numerical computations. *Journal of Ocean Engineering and Marine Energy*, 2:113–127.
- Harris, M., Nicolsky, D., Pelinovsky, E., and Rybkin, A. (2015). Runup of nonlinear long waves in trapezoidal bays: 1-d analytical theory and 2-d numerical computations. *Pure and Applied Geophysics*, 172:885–899.
- Johnson, R. S. (1997). *A Modern Introduction to the Mathematical Theory of Water Waves*. Cambridge University Press.

- Kanoglu, U. (2004). Nonlinear evolution and runup-drawdown of long waves over a sloping beach. *J. Fluid Mech.*, 513:363–372.
- Kanoglu, U. and Synolakis, C. (2006). Initial value problem solution of nonlinear shallow water-wave equations. *Physical Review Letters*, 148501:97.
- Kanoglu, U. and Synolakis, C. (2015). *Coastal and Marine Hazards, Risks, and Disasters*, chapter Tsunami Dynamics, Forecasting, and Mitigation, pages 15–57. Hazards and Disasters Series. ELSEVIER.
- Kanoglu, U., Titov, V., Bernard, E., and Synolakis, C. (2015). Tsunamis: bridging science, engineering and society. *Philosophical Transactions of the Royal Society A*, 373 (2053):20140369.
- Lannes, D. (2013). *The Water Waves Problem: Mathematical Analysis and Asymptotics*, volume 188 of *Mathematical Surveys and Monographs*. American Mathematical Society, Providence, Rhode Island.
- Madsen, P., Fuhrman, D., and Schäffer, H. (2008). On the solitary wave paradigm for tsunamis. *Journal of Geophysical Research; Oceans*, 113.
- Nicolosky, D., Pelinovsky, E., Raza, A., and Rybkin, A. (2018). General initial value problem for the nonlinear shallow water equations: Runup of long waves on sloping beaches and bays. *Physics Letters A*, 382(38):2738–2743.
- NTHMP, editor (2012). *Proceedings and results of the 2011 NTHMP Model Benchmarking Workshop*, NOAA Special Report, Boulder, CO. U.S. Department of Commerce/NOAA/NTHMP, National Tsunami Hazard Mapping Program [NTHMP]. 436 p.
- Pelinovsky, E. (2006). *Hydrodynamics of tsunami waves.*, chapter Waves in Geophysical Fluids (Eds. Grue J. and Trulsen K.), pages 1–48. CISM Courses and Lectures, No. 489. Springer.
- Raz, A., Nicolosky, D., Rybkin, A., and Pelinovsky, E. (2018). Long wave run-up in asymmetric bays and in fjords with two separate heads. *Journal of Geophysical Research, Oceans*, 123(3):2066–2080.
- Rybkin, A., Pelinovsky, E., and Didenkulova, I. (2014). Non-linear wave run-up in bays of arbitrary cross-section:generalization of the Carrier-Greenspan approach. *J. Fluid Mech.*, 748:416–432.

- Stoker, J. (1957). *Water waves: The Mathematical Theory with Applications*. Interscience Publishers.
- Synolakis, C. (1987). The runup of solitary waves. *J. Fluid Mech.*, 185:523–545.
- Synolakis, C. (1991). Tsunami runup on steep slopes: how good linear theory really is? *Natural Hazards*, 4:221–234.
- Synolakis, C. and Bernard, E. (2006). Tsunami science before and beyond Boxing Day 2004. *Philosophical Transactions of the Royal Society A*, 364:2231–2265.
- Synolakis, C., Bernard, E., Titov, V., Kanoglu, U., and Gonzalez, F. (2008). Validation and verification of tsunami numerical models. *Pure Applied Geophysics*, 165:2197–2228.
- Tuck, E. and Hwang, L. (1972). Long wave generation on a sloping beach. *J. Fluid Mech.*, 51:449–461.
- Zahibo, N., Pelinovsky, E., Golinko, V., and Osipenko, N. (2006). Tsunami wave runup on coasts of narrow bays. *International Journal of Fluid Mechanics Research*, 33:106–118.